Purification dynamics in a continuous-time hybrid quantum circuit model

Sebastian Leontica [1,2] and Max McGinley[3,2]

[1]*London Centre for Nanotechnology, University College London, Gordon St., London WC1H 0AH, United Kingdom*
[2]*Rudolf Peierls Centre for Theoretical Physics, Clarendon Laboratory, Parks Road, Oxford OX1 3PU, United Kingdom*
[3]*T.C.M. Group, Cavendish Laboratory, JJ Thomson Avenue, Cambridge CB3 0HE, United Kingdom*

(Received 3 September 2023; revised 30 October 2023; accepted 31 October 2023; published 17 November 2023)

We introduce a continuous-time model of many-body quantum dynamics based on infinitesimal random unitary operations, combined with projective measurements. We consider purification dynamics in this model, where the system is initialized in a mixed state, which then purifies over time as a result of the measurements. By mapping our model to a family of effective 1D quantum Hamiltonians, we are able to derive analytic expressions that capture how the entropy of the system decays in time. Our results confirm the existence of two distinct dynamical phases, where purification occurs over a timescale that is exponential versus constant in system size. We compare our analytic expressions for this microscopic model to results derived from field theories that are expected to capture such measurement-induced phase transitions and find quantitative agreement between the two.

DOI: 10.1103/PhysRevB.108.174308

I. INTRODUCTION

The continuing development of programmable quantum devices with increasing numbers of degrees of freedom has led to a great deal of interest in addressing fundamental questions regarding the dynamics of information in many-body quantum systems [1–12]. In recent years, there has been a particular focus on the competition between unitary operations, which generate entanglement, and local projective measurements, which are nonunitary processes that break entanglement. Models of dynamics that feature both of these ingredients are often referred to as hybrid quantum circuits, the study of which has led to the discovery of a sharp entanglement phase transition driven by the rate of measurements, separating regimes where many-body entanglement is either stable or fragile against these measurements [13–24]. Typically, the studied geometry is that of a 1D chain of qudits, but similar transitions have also been found in more complex geometries such as random tensor networks [25–28]. Interesting behavior of entanglement measures under monitored dynamics has also been recently shown in free fermionic systems, where a Berezinskii–Kosterlitz–Thouless (BKT) type transition between extended criticality and area-law behavior has been suggested [29–33]. The existence and nature of this transition is, however, still the subject of active debate.

The existence of this transition was first understood in terms of the entanglement structure of an ensemble of pure many-body states at equilibrium. Subsequent studies also revealed the existence of a simultaneous dynamical phase transition, which can be understood as the ability of the measurement protocol to learn an initially mixed state [34–37]. The latter suggests a connection between the dynamics of hybrid quantum circuits and quantum error correcting codes [38], which by construction protect information against deleterious nonunitary processes. The transition was also shown to play an important role in the context of simulating the behavior of open quantum systems [39–42].

These considerations have led to the notion of purification dynamics, where one studies how the entropy of an initially mixed state decreases over time as a result of the measurements. Away from the critical measurement rate there are two phases where the state purifies over a timescale that increases exponentially with system size ("mixed phase") or is independent of the system size ("purifying phase") [34]. To understand the phenomenology of these phases in a fully quantitative way, arguments based on capillary wave theory have been put forward [43]. Using an effective field theory which is expected to capture the universal features of the transition, one can obtain concrete predictions of how the purity of the system will depend on time in each phase. However, direct verification of these predictions by means of a direct calculation from a microscopic model are as of yet lacking.

In this paper, we introduce and study a hybrid quantum circuit model of dynamics that is defined in continuous time, the properties of which we are able to calculate analytically. In particular, by means of a mapping onto an effective Hamiltonian, we are able to compute the time dependence of a particular family of operator-space entanglement measurements, which can be related to the purity of the system at a time t, starting from a maximally mixed initial state. For the particular case of the second Rényi entropy and an infinite local dimension of the spin chain, the effective quantum Hamiltonian becomes the well-known transverse field Ising model (TFIM) in imaginary time.

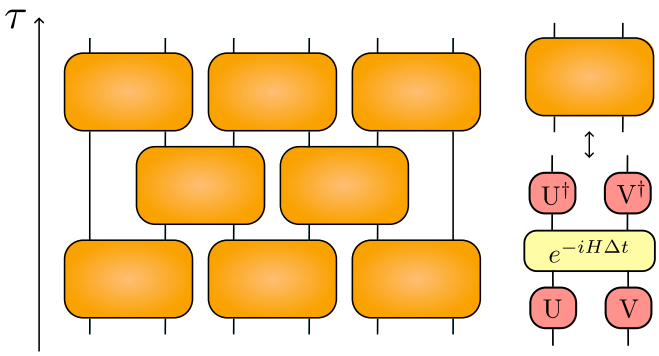

FIG. 1. Schematic representation of the random circuit geometry for open boundary conditions. The construction of the unit cells is illustrated on the right. The Hamiltonian H and evolution time Δt are kept fixed, but the random unitaries U, V are sampled independently at each space-time location in the circuit.

We look in detail at both the mixed and purifying phases, as well as at the transition between them. Our results agree with those of capillary wave theory in both phases: the entropy decays exponentially with time in the purifying phase and decreases as $-\ln t$ in the mixed phase over an exponentially long time window [Eqs. (64) and (71)]. In our calculations, we consider both periodic and open boundary conditions, and show that the two choices give rise to quantitatively different behavior when in the mixed phase: in particular, a $(1/2)\ln N$ contribution to the entropy appears when we impose periodic boundary conditions, but this is absent for open boundary conditions. We also look at the dynamics at criticality, where there exists a regime during which the entropy decays algebraically, Eq. (77).

The structure of our paper is as follows. In Sec. II, we introduce a continuous time model of dynamics based on infinitesimal random unitary operations, and describe how one can calculate various measures of entanglement and information spreading in this model. We supplement the unitary dynamics with projective measurements in Sec. III, and in Sec. IV, we explain how the resultant unitary-projective dynamics can be mapped onto imaginary-time evolution under an effective 1D Hamiltonian. We then present our main quantitative results in Sec. V, giving analytic expressions that quantify how the purity of the system increases as a function of time in the purifying/mixed phase and at criticality. Finally, we discuss our results and conclude in Sec. VI.

II. CONTINUOUS-TIME RANDOM CIRCUIT MODEL

In this section, we introduce a random unitary circuit (RUC) model of unitary dynamics, and describe how its entanglement properties can be analysed. We will later incorporate measurements into this model, which will allow us to study the dynamics of purification.

We consider a one-dimensional array of N qudits, each with a local Hilbert space of dimension d. The evolution is driven by a spatially local unitary circuit with a brickwork structure, illustrated in Fig. 1. In a given timestep $\tau = 1, 2, \ldots$, two-site unitaries are applied to each pair of qudits on the odd bonds $(2j-1, 2j)$, followed by another layer of unitaries on the even bonds $(2j, 2j+1)$. These elementary two-site unitaries each have the same structure, also depicted in Fig. 1. First, single-site gates $U \otimes V$ are applied, followed by evolution under some two-qudit Hamiltonian H for a time Δt, and finally the change of basis is undone by applying the inverse single-site rotations $U^\dagger \otimes V^\dagger$. We denote the unitary operator describing the evolution from time 0 to τ as $W(\tau)$.

Throughout this work, H will be treated as a free parameter of the model and it is kept fixed across both time and space. To simplify calculations, we will assume it is real, hermitian and symmetric under swapping the two qudits it acts on. The single-qudit unitaries will be sampled randomly and independently from the Haar ensemble for each unit cell. We will generally be interested in the limit where $\Delta t \to 0$, which we refer to as the continuous-time limit. Note that the state only evolves by an infinitesimal amount in each timestep, in contrast to discrete-time RUC models of quantum dynamics (e.g., Refs. [6,11]). A model of continuous-time dynamics was studied numerically in Ref. [44]. Our method for constructing the unit cell is more general and more easily amenable to analytical treatment.

The model was chosen with two main principles in mind. The first is that infinitesimal transformations commute up to quadratically small error terms due to the Trotter formula. This means we do not need to worry about the alternating layers in the brickwork circuit and should expect the final evolution to be uniform in time. The second is to introduce Haar random rotations in a way that simplifies calculations without affecting the first condition. The unit cell we propose satisfies both criteria, while still allowing for a large degree of generality through the free matrix parameter H. In this work we keep it constant, but the discussion could be generalized in a straightforward way to include dependence of H on both time and space.

Our focus will be on the dynamics of entanglement and quantum information in these continuous-time models. For this purpose, it is useful to consider the Choi-Jamiolkowski (CJ) state $|W(\tau)\rangle$ corresponding to the unitary $W(\tau)$. This state is defined on two copies of the system, which we can associate with the inputs and outputs of the time evolution operator. Formally, we have $|W(\tau)\rangle = [\mathbb{I} \otimes W(\tau)]\,|\Phi^+\rangle$, where $|\Phi^+\rangle = \bigotimes_{j=1}^{N}(d^{-1/2}\sum_{a=1}^{d}|a\rangle \otimes |a\rangle)$ consists of maximally entangled states between each input qudit and its corresponding output [45]. Many important quantities that are used to diagnose the spreading of quantum information can be expressed as simple functions of this operator state $|W(\tau)\rangle$ [5].

As is now common in studies of RUC dynamics, we use the Rényi entropies to quantify the entanglement properties of the state $|W(\tau)\rangle$

$$S^{(n)}(\rho_A) = \frac{1}{1-n}\ln \mathrm{tr}\left(\rho_A^n\right), \tag{1}$$

where n is some positive parameter. Here, ρ_A is the reduced density matrix of $|W(\tau)\rangle$ corresponding to some subset A of inputs and outputs. Compared to the usual von Neumann entropy S_{vN}, the Rényi entropies for $n = 2, 3, \ldots$ are more amenable to analytic studies, since they only involve integer moments of the density matrix and hence can be computed using a replica method. The von Neumann entanglement entropy S_{vN} can be recovered by constructing an analytical continu-

ation of the function and taking the limit $n \to 1$ (see, e.g., Ref. [46]).

For the largest part of this work, we will only be concerned with the second Rényi entropy $S^{(2)}(\rho_A)$, which is the simplest to evaluate. This is a lower bound on the von Neumann entropy $S_{\text{vN}} \geqslant S^{(2)}$, which in certain cases is known to be asymptotically tight [47]. Since the purity $\text{Tr}[(\rho^A)^2] \equiv \exp[-S^{(2)}(\rho^A)]$ is a quadratic function of $|W(\tau)\rangle\langle W(\tau)|$, it can be expressed using a fourfold copy of the evolution operator, which we denote

$$\mathbf{W}^{(2)}(\tau) \coloneqq (W(\tau) \otimes W^*(\tau))^{\otimes 2}. \tag{2}$$

Note here that the operator replicated in the expression differs from $|W(\tau)\rangle\langle W(\tau)|$ by a reshuffling of the indices. Henceforth, we will use this convention, but retain the essence of the CJ isomorphism by noting that we treat inputs and outputs on par when discussing Rényi entropies.

Define (unnormalized) states

$$|\mathbf{I}\rangle_j = \sum_{a,b=1}^{d} (|a\rangle \otimes |a\rangle \otimes |b\rangle \otimes |b\rangle)_j, \tag{3}$$

$$|\mathbf{S}\rangle_j = \sum_{a,b=1}^{d} (|a\rangle \otimes |b\rangle \otimes |b\rangle \otimes |a\rangle)_j, \tag{4}$$

which live in the fourfold-replicated Hilbert space of each physical site j. In terms of these, we have

$$e^{-S^{(2)}} = \text{Tr}[(\rho^A)^2] = \langle \Psi_{A_{\text{out}}} | \mathbf{W}^{(2)}(\tau) | \Psi_{A_{\text{in}}} \rangle , \tag{5}$$

where we denote the set of input (output) sites included in the region A as A_{in} (A_{out}), and the states

$$|\Psi_{A_{\text{in}}}\rangle = \left(\bigotimes_{j \in A_{\text{in}}} |\mathbf{S}\rangle_j \right) \otimes \left(\bigotimes_{j \notin A_{\text{in}}} |\mathbf{I}\rangle_j \right), \tag{6}$$

and similar for $|\Psi_{A_{\text{out}}}\rangle$.

To make progress, we look at the average of the Rényi entropy (5) over the random ensemble of unitary circuits. More precisely, we will evaluate the average purity as opposed to the average entropy, which is equivalent to performing averages inside the logarithm of Eq. (1). This simplification is common in analyses of RUCs [17], and still recovers the correctly-averaged von Neumann entropy if one takes the replica limit $n \to 1$. Accordingly, averaging the purity amounts to replacing $\mathbf{W}^{(2)}(\tau)$ with its ensemble average $\overline{\mathbf{W}^{(2)}(\tau)}$. As shown in Appendix I in Ref. [48], $\overline{\mathbf{W}^{(2)}(\tau)}$ maps states spanned by tensor products of $|\mathbf{I}\rangle_j$, $|\mathbf{S}\rangle_j$ to other such states, meaning we can focus on the restriction of this averaged operator to the subspace $V(S_2)^{\otimes N}$, where $V(S_2) = \text{span}(|\mathbf{I}\rangle , |\mathbf{S}\rangle)$.

Because the single-site Haar-random unitaries appearing in each of the two-site elementary blocks of the circuit (Fig. 1) are sampled independently, we can consider the ensemble average of the evolution under a single one of these blocks, which we denote $\mathcal{T} : V(S_2)^{\otimes 2} \to V(S_2)^{\otimes 2}$. Using the Weingarten diagrammatic calculus as seen in Appendix I in Ref. [48], we find that, for small Δt, this map can be expressed as

$$\mathcal{T}_{ij} = 1 - \Delta t^2 \Omega(H) \mathcal{W}g^{(i)} \mathcal{W}g^{(j)} \left(1 - \sigma_z^{(i)} \sigma_z^{(j)}\right) + \mathcal{O}(\Delta t^4), \tag{7}$$

where i, j label the sites on which the unit cell acts, $\Omega(H)$ is a measure of the entangling power of the Hamiltonian

$$\Omega(H) = d^2 \,\text{tr}(H^2) - 2d \,\text{tr}(\text{tr}_1(H)^2) + \text{tr}(H)^2, \tag{8}$$

and $\mathcal{W}g$ is the Weingarten matrix corresponding to the symmetric group S_2

$$\mathcal{W}g = \frac{1}{d(d^2-1)} \begin{bmatrix} d & -1 \\ -1 & d \end{bmatrix} = \frac{1}{d^2-1} \left(1 - \frac{\sigma_x}{d}\right). \tag{9}$$

The induced evolution can be equivalently described using the effective imaginary-time Hamiltonian

$$\mathcal{H}_{ij} = \Omega(H) \mathcal{W}g^{(i)} \mathcal{W}g^{(j)} \left(1 - \sigma_z^{(i)} \sigma_z^{(j)}\right), \tag{10}$$

in terms of which the unit cell map is

$$\mathcal{T}_{ij} = e^{-\Delta t^2 \mathcal{H}_{ij}} + \mathcal{O}(\Delta t^4). \tag{11}$$

It is interesting to note that there are no contributions from odd powers of Δt in the expansion of Eq. (7). Looking at the form of the Hamiltonian (10), we see that in the effective Hilbert space spanned by the states (3) and (4), the only mobile degrees of freedom are domain walls separating regions of $|\mathbf{I}\rangle$ from $|\mathbf{S}\rangle$, consistent with discrete-time RUCs discussed previously [6,11]. The initial Hamiltonian H only enters the expression through its entangling rate $\Omega(H)$. This sets the overall timescale of quantum information transfer through the system. In Appendix II in Ref. [48], we compute the transfer matrix for a higher number of replicas and show that this statement holds more generally. This result suggests that the qualitative behavior of entanglement dynamics derived from our model should be insensitive to most of the microscopic details, and hence applicable to a wide range of physical processes.

The propagator for the whole circuit $\mathcal{T}$ can be constructed by concatenating the two-site maps (11) according to the brickwork circuit structure illustrated in Fig. 1. We have

$$\mathcal{T}(\tau) = \left(\prod_{\substack{i=2 \\ i \,\text{even}}}^{N-2} e^{-\Delta t^2 \mathcal{H}_{i,i+1}} \prod_{\substack{i=1 \\ i \,\text{odd}}}^{N-1} e^{-\Delta t^2 \mathcal{H}_{i,i+1}} \right)^{\tau} + \mathcal{O}(\tau \Delta t^4). \tag{12}$$

We now define the effective time as $t = \tau \Delta t^2$ and take the limit $\tau \to \infty$, $\Delta t \to 0$ such that t is kept constant. Using the Suzuki-Trotter formula, we find the limit of the previous equation

$$\mathcal{T}(t) = \exp\left(-t \sum_{i=1}^{N-1} \mathcal{H}_{i,i+1} \right). \tag{13}$$

We reiterate here that this operator acts as the restriction of $\overline{\mathbf{W}^{(2)}(\tau)}$ to its invariant subspace $V(S_2)^{\otimes N}$ and therefore may replace it in average entropy calculations [e.g., averaging Eq. (5)].

In its current form, the effective Hamiltonian $\sum_{i=1}^{N-1} \mathcal{H}_{i,i+1}$ is not Hermitian, but can be made so through a local similarity transformation, a technique commonly encountered in the study of nonequilibrium dynamics [49]. If we define a new evolution operator by $\tilde{\mathcal{T}} = (\mathcal{W}g^{-\frac{1}{2}})^{\otimes N} \mathcal{T} (\mathcal{W}g^{\frac{1}{2}})^{\otimes N}$, each 2-local term in the effective Hamiltonian transforms as

$\tilde{\mathcal{H}}_{ij} = (\mathcal{W}g^{-\frac{1}{2}})^{\otimes 2}\mathcal{H}_{ij}(\mathcal{W}g^{\frac{1}{2}})^{\otimes 2}$, which gives us the Hermitian interaction

$$\tilde{\mathcal{H}}_{ij} = \frac{\gamma}{2}\Big[1 - \frac{d^2-1}{d^2}\sigma_z^{(i)}\sigma_z^{(j)} + \frac{1}{d^2}\sigma_x^{(i)}\sigma_x^{(j)} - \frac{1}{d}\big(\sigma_x^{(i)} + \sigma_x^{(j)}\big)\Big], \tag{14}$$

where the overall strength is given by $\gamma = 2\Omega(H)/(d^2-1)^2$. This type of local interaction is found in the literature both as the quantum equivalent of the classical two-dimensional axial next-nearest neighbor Ising model (ANNNI) [50,51] or more recently as the Jordan-Wigner transform of the balanced interacting Kitaev chain [52,53].

In the limit of $d \to \infty$, we are left with a simple ferromagnetic nearest-neighbor Hamiltonian, with each domain wall incurring an energy penalty of γ. The Hamiltonian is symmetric under the global spin-flip operator $\mathcal{C} = \prod_i \sigma_x^{(i)}$, as can be seen through the commutation relation $[\mathcal{C}, \mathcal{H}_{ij}] = 0$.

III. INCLUDING MEASUREMENTS

In this section, we will introduce the formalism that can be used to incorporate measurements into the random circuit evolution. For the purpose of this work, we will consider projective measurements in the computational basis of each qudit that occur stochastically. The same framework can accommodate for weak-measurement schemes as seen in Ref. [17]. Due to the continuous nature of our circuits, the effective model will be identical in the two cases.

A projective measurement is a nonunitary stochastic process, where the wave function of the system $|\psi\rangle$ collapses to a postmeasurement state $|m\rangle$ with probability $p_m = |\langle m|\psi\rangle|^2$. Here, the set of wave functions $\{|m\rangle\}$ is the computational basis in which the measurement is performed and $m = 1, 2, \ldots d$. For any fixed realization of the random unitary circuit and positioning of the measurements, the final state of the system will depend on all the measurement outcomes $\mathbf{m} = (m_1, m_2, \ldots)$. Thus we can write the ensemble of final states as $\{(p_{\mathbf{m}}, |W_{\mathbf{m}}\rangle)\}$, where $p_{\mathbf{m}}$ is the joint probability of the measurement results, and $|W_{\mathbf{m}}\rangle$ is the (normalized) conditional state. As before, we will imagine the Choi-Jamiolkowski state, so $|W_{\mathbf{m}}\rangle$ is a state on a twofold copy of the system, and is constructed by preparing a maximally entangled state between the two copies in the computational basis, and evolving one of the copies under the evolution in question.

As is typical in the study of hybrid quantum circuits, our interest is on the statistics of the entanglement properties of individual conditional wave functions $|W_{\mathbf{m}}\rangle$; see, e.g., Refs. [14,34]. The natural quantity to consider for this purpose is the von Neumann entropy, $S_{\mathrm{vN}}(\rho_{\mathbf{m}}^A)$, where $\rho_{\mathbf{m}}^A$ is the reduced density matrix of $|W_{\mathbf{m}}\rangle$ over a subset of inputs and outputs A. Specifically, we would want to compute the average of this quantity over all realizations of the random circuit, measurement locations and measurement results, which we denote $\overline{S_{\mathrm{vN}}(\rho_{\mathbf{m}}^A)}$. However, this quantity is very difficult to compute directly in random circuit models. We follow Ref. [17] and introduce the series of related quantities

$$\tilde{S}_A^{(n)} = \frac{1}{1-n}\ln\left|\frac{\sum_{\{M\}} p_M d^{|M|(n-1)}\overline{\sum_{\mathbf{m}} p_{\mathbf{m}}^n \operatorname{tr}[(\rho_{\mathbf{m}}^A)^n]}}{\sum_{\{M\}} p_M d^{|M|(n-1)}\overline{\sum_{\mathbf{m}} p_{\mathbf{m}}^n}}\right|, \tag{15}$$

where M labels a particular configuration of measurement locations in space-time, which occurs with probability p_M, and $\mathbf{m}$ runs over all measurement results for the given configuration M. These quantities are related to measurement-averaged Rényi entropies, with the main difference that each outcome is weighted by $p_{\mathbf{i}_M}^n$. The additional factor of $d^{|M|(n-1)}$ ensures that the correct order of magnitude, in powers of d, of the correct weight is preserved, and only deviations from it are amplified by the number of replicas. The renormalization is also performed on average, i.e., we compute the average of the numerator and the denominator independently. Knowledge of this quantity for all integers $n \geqslant 2$ can be used to recover the average entanglement entropy $\overline{S_A}$ of subsystem A using the replica limit

$$\overline{S_{\mathrm{vN}}(\rho_{\mathbf{i}}^A)} = \lim_{n\to 1}\tilde{S}_A^{(n)}. \tag{16}$$

Each term in the sums over M appearing in the numerator and the denominator in Eq. (15) is a scalar that depends linearly on the tensor

$$\overline{\langle \mathbf{W}^{(n)}\rangle} = d^{|M|(n-1)}\overline{\sum_{\mathbf{m}} p_{\mathbf{m}}^n (W_m \otimes W_m^*)^{\otimes n}}, \tag{17}$$

which is analogous to the duplicated state in Eq. (2) defined earlier. The angled brackets are a short-hand notation for the weighted sum on the RHS. For simplicity, we once again revert to the normal operator indices, but keep in mind that the probabilities are obtained from expectation values of the appropriate projectors in the CJ state $|W_m\rangle$.

To see how this tensor evolves as the circuit progresses, let us consider how $\overline{\langle \mathbf{W}^{(n)}\rangle}$ is updated when a new measurement is performed on site i, the outcome of which we denote m. Each of the n replicas transforms via the action of a projector $P_m^{(i)}$, which corresponds to the mth computational basis state for qudit i. Since all measurement outcomes m are summed over in Eq. (17), we find

$$\overline{\langle \mathbf{W}^{(n)}\rangle} \to d^{n-1}\mathcal{M}_i(\overline{\langle \mathbf{W}^{(n)}\rangle}) = d^{n-1}\sum_m \big(P_m^{(i)}\big)^{\otimes 2n}\overline{\langle \mathbf{W}^{(n)}\rangle}. \tag{18}$$

The effect of postselection is included by assuming a perfect correlation of the measurement results in all n replicas.

Since adding an infinitesimal time evolution to the averaged tensor only leads to linear transformations by left multiplication due to both the chaotic dynamics and the measurements, we can proceed again by mapping the evolution of $\overline{\langle \mathbf{W}^{(n)}\rangle}$ to a reduced system with an effective Hamiltonian. If we focus again on the twofold replica $n = 2$, we see that the action of the measurement operator on the reduced Hilbert

space at each site is

$$\mathcal{M}\,|\mathbf{I}\rangle = d\sum_m P_m^{\otimes 4}\,|\mathbf{I}\rangle = d\sum_m |m\rangle^{\otimes 4} := |\mathbf{O}\rangle\,,$$
$$\mathcal{M}\,|\mathbf{S}\rangle = d\sum_m P_m^{\otimes 4}\,|\mathbf{S}\rangle = |\mathbf{O}\rangle\,,$$
$$\mathcal{M}\,|\mathbf{O}\rangle = d\sum_m P_m^{\otimes 4}\sum_n |n\rangle^{\otimes 4} = |\mathbf{O}\rangle\,. \tag{19}$$

Therefore we find that the new vector space $V_{\mathcal{M}}(S_2) = \mathrm{span}(|\mathbf{I}\rangle, |\mathbf{S}\rangle, |\mathbf{O}\rangle)$ is closed under measurements. If we promote this to the reduced Hilbert space of the entire chain $V_{\mathcal{M}}^{\otimes N}(S_2)$, we find that this is also closed under the action of the Haar averaged unit cell between any pair of sites. To show this, we can consider the properties of the following linear combination

$$|\mathbf{X}\rangle := |\mathbf{O}\rangle - \frac{d}{d+1}(|\mathbf{I}\rangle + |\mathbf{S}\rangle) \in V_{\mathcal{M}}(S_2). \tag{20}$$

It is straightforward to show that this becomes null under any contraction between a normal and a complex conjugate leg. Due to the rules of the Weingarten calculus, this means that such local states are preserved by averaged unit cells. This is summarized in the following equation

$$\mathcal{T}_{ij}^{\mathcal{M}}\,|\mathbf{X}\rangle \otimes V_{\mathcal{M}}(S_2) \in |\mathbf{X}\rangle \otimes V_{\mathcal{M}}(S_2). \tag{21}$$

In Appendix III in Ref. [48] we give an explicit representation of the new operator $\mathcal{T}_{ij}^{\mathcal{M}}$, acting on $V_{\mathcal{M}}(S_2)^{\otimes 2}$. We find that evolution in subspaces that contain $|\mathbf{X}\rangle$ states happen at a different rate Γ, independent of the rate of information propagation γ. This is defined by

$$\Gamma = \frac{2d}{(d^2-1)^2}\,\mathrm{tr}(\mathrm{tr}_1(H)^2), \tag{22}$$

and can be qualitatively understood as an energy cost associated with $|\mathbf{X}\rangle$ states. In Appendix IV in Ref. [48] (see also Ref. [54] therein) we derive a more explicit relation between the rates Γ, γ and the microscopic Hamiltonian H.

The new state $|\mathbf{X}\rangle$, which appears after a measurement, ensures that we obtain the correct correlations between measurements performed consecutively at short time intervals on the same qudit. The timescale $1/\Gamma$ represents the time it takes a qudit to relax before we can obtain new information by measuring again in the same basis. For the rest of this work, we set $\Gamma \to \infty$, such that no measurement inertia can be observed. In Appendix III in Ref. [48], we show that doing so is effectively equivalent to projecting out the $|\mathbf{X}\rangle$ state and working in the previous two-dimensional reduced Hilbert space $V(S_2)$. The action of the measurements is also projected onto this subspace and can be expressed as

$$\mathcal{M} = \frac{d}{d+1}(1+\sigma_x). \tag{23}$$

It can be shown that this same operator is obtained in the reduced subspace if we consider instead measurements in random bases.

In the following, the measurements are distributed through the circuit according to an independent Poisson process for each site, at some uniform rate f (in the natural time units of the continuous model). The transfer matrix at time t under both random dynamics and measurements is then given by an effective imaginary-time evolution $\mathcal{T}_{\mathrm{eff}}(t) = \exp(-t\mathcal{H}_{\mathrm{eff}})$, with $\mathcal{H}_{\mathrm{eff}}$ given by

$$\mathcal{H}_{\mathrm{eff}} = \sum_{i=1}^{N-1}\mathcal{H}_{i,i+1} - f\sum_{i=1}^{N}(\mathcal{M}_i - 1). \tag{24}$$

From Eqs. (5) and (15), we see that we can express the second moment of the entanglement entropy of some subregion A at time t using matrix elements of the transfer matrix

$$\tilde{S}_A^{(2)} = -\ln\left|\frac{\langle\Psi_{A_{\mathrm{out}}}|\,\mathcal{T}_{\mathrm{eff}}(t)\,|\Psi_{A_{\mathrm{in}}}\rangle}{\langle\mathbf{I}|^{\otimes N}\,\mathcal{T}_{\mathrm{eff}}(t)\,|\Psi_{A_{\mathrm{in}}}\rangle}\right|. \tag{25}$$

The denominator acts as a normalization factor, so using the expression above allows us to safely drop constant terms in the effective Hamiltonian.

We can perform a similar analysis for the case of multiple replicas. Using the results in Appendix II in Ref. [48] and the limits $d, \Gamma \to \infty$ we show that the effective Hamiltonian of the n'th replica theory is given by

$$\mathcal{H}_{\mathrm{eff}}^{(n)} = \frac{\gamma}{2}\sum_{i=1}^{N-1} D_{ij} - f\sum_{i=1}^{N}\mathcal{M}^{(n)}, \tag{26}$$

where $\mathcal{M}^{(n)}$ is the generalization of the operator in Eq. (23) that acts as

$$\mathcal{M}^{(n)}\,|\tau\rangle = \sum_{\sigma\in S_n}|\sigma\rangle\,, \tag{27}$$

and D is a diagonal two-site operator with entries given by

$$D_{\kappa\epsilon,\sigma\tau} = \delta_{\kappa\sigma}\delta_{\epsilon\tau}D(\sigma,\tau), \tag{28}$$

with $D(\sigma,\tau)$ the bi-invariant metric on S_n given by the Hamming distance between σ and τ, i.e., the number of elements that are not mapped onto themselves under $\tau^{-1}\sigma$. This form is manifestly consistent with the expected symmetry group $S_n \times S_n$. It is interesting to note that the $d \to \infty$ limit does not result in the fine tuned $S_{n!}$-symmetric Potts model observed in circuits with fully Haar random unit cells [17].

IV. FERMIONIC MAPPING

If we take the limit of large local dimension d and keep only the leading contributions, we obtain dynamics driven by

$$\mathcal{H}_{\mathrm{eff}} = -\frac{\gamma}{2}\left(\sum_{i=1}^{N-1}\sigma_z^{(i)}\sigma_z^{(i+1)} + g\sum_{i=1}^{N}\sigma_x^{(i)}\right), \tag{29}$$

where $g = 2f/\gamma$. This is easily recognized as the transverse field Ising model (TFIM) in 1D, subject to open boundary conditions. It is well-known that this can be mapped to a system of noninteracting fermions using the Jordan-Wigner transformation [55]. In this section, we will introduce the general formalism used to compute quantities of the form shown in Eq. (25).

We start by constructing a set of nonlocal Majorana operators as

$$\gamma_i^{(1)} = \sigma_z^{(i)} \prod_{j>i} \sigma_x^{(j)}, \tag{30}$$

$$\gamma_i^{(2)} = \sigma_y^{(i)} \prod_{j>i} \sigma_x^{(j)} = -i\sigma_z^{(i)} \prod_{j\geqslant i} \sigma_x^{(j)}, \tag{31}$$

defined on all sites $i = 1, 2, \ldots, N$ [56]. These operators are Hermitian $(\gamma^\mu)^\dagger = \gamma^\mu$ and obey the standard anticommutation relations

$$\{\gamma^\mu, \gamma^\nu\} = 2\delta^{\mu\nu}, \tag{32}$$

where the indices μ, ν are understood to run over all $2N$ previously defined operators. From the definition, we get the additional relation

$$\gamma_i^{(1)}\gamma_i^{(2)} = -i\sigma_x^{(i)}, \tag{33}$$

such that the product of all Clifford operators is

$$\prod_{i=1}^{N} \gamma_i^{(1)}\gamma_i^{(2)} = (-i)^N \prod_{i=1}^{N} \sigma_x^{(i)} := (-i)^N \mathcal{C}. \tag{34}$$

This operator anticommutes with all the Majorana fermions $\{\mathcal{C}, \gamma^\mu\} = 0$ and it is a conserved quantity, since it commutes with the full Hamiltonian $[\mathcal{C}, \mathcal{H}] = 0$. We can couple Majorana fermions living on adjacent sites into domain wall creation and annihilation operators

$$a_i^\dagger = \tfrac{1}{2}\big(\gamma_i^{(1)} - i\gamma_{i+1}^{(2)}\big), \tag{35}$$

$$a_i = \tfrac{1}{2}\big(\gamma_i^{(1)} + i\gamma_{i+1}^{(2)}\big), \tag{36}$$

for $i = 0, 1, \ldots, N-1$, where we assume periodic boundary condition $N = 0$. These obey the typical anticommutation relations

$$\{a_i, a_j\} = 0, \quad \{a_i^\dagger, a_j^\dagger\} = 0, \quad \{a_i, a_j^\dagger\} = \delta_{ij}. \tag{37}$$

A simple calculation shows that

$$a_i^\dagger a_i = \tfrac{1}{2}\big(1 - \sigma_z^{(i)}\sigma_z^{(i+1)}\big), \tag{38}$$

such that the number operator of the fermionic mode at some site $i \neq 0$ is a projector onto configurations that have a domain wall between sites i and $i+1$. With this convention, the Hamiltonian becomes a quadratic form

$$\mathcal{H}_{\text{eff}} = \frac{\gamma}{2}\left[\sum_{i=1}^{N-1} a_i^\dagger a_i - g\sum_{i=1}^{N}(a_i^\dagger + a_i)(a_{i-1} - a_{i-1}^\dagger)\right]. \tag{39}$$

This can be more succinctly expressed using the Bogoliubov-de Gennes notation

$$\mathcal{H}_{\text{eff}} = \tfrac{1}{2}\mathbf{a}^\dagger \mathcal{D}\mathbf{a}, \tag{40}$$

where $\mathbf{a} = (a_0, a_1, \ldots, a_{N-1}, a_0^\dagger, a_1^\dagger, \ldots, a_{N-1}^\dagger)^T$. The matrix $\mathcal{D}$ is called the grand-dynamical matrix and it obeys the particle-hole symmetry equation

$$\eta\mathcal{D}^T\eta = -\mathcal{D}, \quad \text{where} \quad \eta = \begin{bmatrix} 0 & I \\ I & 0 \end{bmatrix}. \tag{41}$$

The exponentials of such Hamiltonians are most easily treated using the algebra of fermionic Gaussian states, as worked out in Ref. [57]. We will briefly outline some of the results relevant to our calculation. It is convenient to define a Gaussian state through its generating quadratic form as

$$\rho[W] = \frac{1}{Z(W)} \exp\left(\frac{1}{2}\mathbf{a}^\dagger W \mathbf{a}\right), \tag{42}$$

with a normalization constant $Z(W)$ chosen such that $\text{Tr}\rho[W] = 1$. By Wick's theorem, such many-body states are fully characterized by their two-body correlation matrix, defined as

$$\Gamma_{\mu\nu} = 2\text{Tr}(\rho[W]\mathbf{a}_\mu^\dagger \mathbf{a}_\nu) - \delta_{\mu\nu}. \tag{43}$$

The correlation matrix is related to the generator of the quadratic form through the useful relations

$$\Gamma = \tanh\left(\frac{W}{2}\right), \quad e^W = \frac{1+\Gamma}{1-\Gamma}, \tag{44}$$

where it is assumed that $1 - \Gamma$ is invertible. Using a special case of the Baker-Campbell-Hausdorff formula, it is shown that fermionic Gaussian states are closed under multiplication and we have

$$\rho[\Omega] = \frac{Z(W)Z(W')}{Z(\Omega)}\rho[W]\rho[W'], \tag{45}$$

with the new generating matrix Ω given by

$$\Omega = \ln(\exp(W)\exp(W')). \tag{46}$$

If we denote the correlation matrix of Ω by $\Gamma \times \Gamma'$, with Γ and Γ' the correlation matrices of W and W' respectively, the following formula is proven in Ref. [57]

$$\Gamma \times \Gamma' = 1 - (1-\Gamma')\frac{1}{1+\Gamma\Gamma'}(1-\Gamma). \tag{47}$$

Inner products can be easily computed using the following trace formula

$$\{\Gamma, \Gamma'\} = \text{Tr}(\rho[W]\rho[W']) = \pm\sqrt{\left|\det\frac{1+\Gamma\Gamma'}{2}\right|}, \tag{48}$$

where the ambiguity of the sign is in general a complex issue, but this will not be a problem for our purposes.

V. DYNAMICS OF PURIFICATION

In the preceding sections, we developed a formalism that allows us to study entanglement dynamics in our continuous-time random quantum circuit models. Here, we focus specifically on purification dynamics in these models. Namely, starting from an initial mixed state, we are interested in how fast the state of the system is purified by measurements. We will be particularly interested in the purification transition that occurs as a function of measurement frequency f [34], which is thought to be concomitant with the measurement-induced entanglement transition separating area- and volume-law phases [13–16,18]. Thanks to the exact solvability of our model in the $d \to \infty$ limit, we are able to compute analytical expressions for the order parameters of this dynamical phase transition, and infer the key critical exponents.

A. Setup and phase diagram

The setup we study is as in Ref. [34]: the system is initialized in a maximally mixed state, which is represented in the above formalism by the input state $|\mathbf{I}\rangle^{\otimes N}$. After some evolution time t, the purity of the state of the system will have increased from its initial value due to the measurements. As explained previously, we will use the quantity (15) as a measure of the typical entropy of the ensemble of states. Since we are looking at the purity of the entire state after a time t, the set A that appears in Eq. (25) will contain all of the output qubits. Accordingly, we can express the quantity in question in terms of the transfer matrix $\mathcal{T}_{\text{eff}}(t)$

$$\tilde{S}^{(2)}(t) = -\ln\left|\frac{\langle\mathbf{S}|^{\otimes N}\,\mathcal{T}_{\text{eff}}(t)\,|\mathbf{I}\rangle^{\otimes N}}{\langle\mathbf{I}|^{\otimes N}\,\mathcal{T}_{\text{eff}}(t)\,|\mathbf{I}\rangle^{\otimes N}}\right|. \tag{49}$$

The purification transition that occurs in our model is associated with a quantum phase transition in the effective Hamiltonian $\mathcal{H}_{\text{eff}}$, which generates the time evolution operator $\mathcal{T}_{\text{eff}}(t)$. Based on the phase diagram of the TFIM, we can deduce that such a transition must occur at the critical measurement rate $g_c = 1$, i.e., $f_c = \gamma/2$. In the spin basis (29), the two phases correspond to the $\mathbb{Z}_2$ symmetric phase under the symmetry $\mathcal{C} = \prod_{i=1}^{N}\sigma_x^{(i)}$ for $g > 1$, and a spontaneous symmetry-broken phase for $g < 1$.

For the problem in hand, the relevant order parameter that we use to distinguish the two phases is not a correlation function, as is usually the case, but rather the many-body overlap appearing inside the logarithm in Eq. (49). We also note in passing that the numerator and denominator inside the logarithm in Eq. (49) are reminiscent of the many-body overlap amplitudes that appear in dynamical quantum phase transitions (DQPTs). DQPTs in the TFIM have been thoroughly investigated [58,59], although we note that the quantities we are interested in here differ in that the evolution is in imaginary time, and for the numerator the initial and final states are not the same. For this reason, we cannot immediately lift results from that context.

To provide intuition into how this quantity behaves either side of the transition, we can reformulate our expression for $\tilde{S}^{(2)}(t)$ as follows. Since $|\mathbf{S}\rangle^{\otimes N} = \mathcal{C}\,|\mathbf{I}\rangle^{\otimes N}$, the above fraction becomes equal to the expectation value of $\mathcal{C}$ in the state $|\Psi(t)\rangle = \mathcal{T}_{\text{eff}}^{\frac{1}{2}}|\mathbf{I}\rangle^{\otimes N}$, namely,

$$\tilde{S}^{(2)}(t) = -\ln|\langle\mathcal{C}\rangle_{\tilde{\Psi}(t)}|, \tag{50}$$

where $|\tilde{\Psi}(t)\rangle := |\Psi(t)\rangle/\sqrt{\langle\Psi(t)|\Psi(t)\rangle}$ is the wave function after imaginary time evolution under $\mathcal{H}_{\text{eff}}/2$, appropriately normalized.

If the measurement rate is sufficiently high such that the Hamiltonian (29) is in a symmetry-unbroken phase, then the ground state is nondegenerate and thus $|\tilde{\Psi}(t)\rangle$ inherits the symmetry of the Hamiltonian. Since the Hamiltonian is also gapped, we see that the (accordingly normalized) state $|\Psi(t)\rangle = \exp(-t\mathcal{H}_{\text{eff}}/2)\,|\mathbf{I}\rangle^{\otimes N}$ converges to the ground state exponentially quickly. The ground state must be an eigenstate of $\mathcal{C}$, whose eigenvalues are ± 1, so we can then conclude that $|\langle\mathcal{C}\rangle_{\tilde{\Psi}(t)}| \to 1$ exponentially quickly as $t \to \infty$, and hence $\tilde{S}^{(2)} \to 0$ at a rate independent of the system size, as expected in this regime. When $g < 1$ the symmetry is spontaneously broken. In this case, the ground eigenspace is doubly degenerate in the thermodynamic limit $N \to \infty$, and the effect of the transfer matrix at long times is to project onto this subspace. The projected state may no longer be an eigenstate of $\mathcal{C}$, so we can have a nonzero residual entropy. As we will see, this residual entropy is extensive, with a $\ln(N)$ correction [Eq. (69)].

While this picture allows us to understand the transition at a qualitative level, to obtain an analytic expression for the residual entropy, we will instead use the fermionic mapping detailed in the previous section. We will find it convenient to work with states of definite fermion parity, and hence we define the density matrices $\rho_\pm = |\pm\rangle\langle\pm|$, where $|\pm\rangle := (|\mathbf{I}\rangle^{\otimes N} \pm |\mathbf{S}\rangle^{\otimes N})/\sqrt{2}$, which are eigenstates of $\mathcal{C}$. We can then write

$$\tilde{S}^{(2)} = \ln\left|\frac{1+\Theta}{1-\Theta}\right|, \tag{51}$$

where the parameter Θ is defined by

$$\Theta = \frac{\text{Tr}(e^{-t\mathcal{H}_{\text{eff}}}\rho_+)}{\text{Tr}(e^{-t\mathcal{H}_{\text{eff}}}\rho_-)}, \tag{52}$$

We note that Eqs. (51) and (52) are quite general, and could be applied even if we didn't take the $d \to \infty$ limit.

Because the Hamiltonian (39) is a fermion bilinear, the exponential $e^{-t\mathcal{H}_{\text{eff}}}$ can be written in the form of Eq. (42), with the grand dynamical matrix $\mathcal{D}$ in place of W. Hence we can define correlation matrices $\Gamma[-t\mathcal{D}]$ that correspond to this fermionic state, according to Eq. (43). The states $\rho_\pm$ are also Gaussian fermionic states, and hence can be characterized through their correlation matrices. These have the simple diagonal form $\Gamma_{GS} = \text{diag}(-1, -1, \ldots, -1, 1, 1, \ldots, 1)$ and $\Gamma_E = \text{diag}(1, -1, \ldots, -1, -1, 1, \ldots, 1)$, with ± 1 each appearing N times. Then, using Eq. (48) we obtain

$$\Theta = \frac{\{\Gamma[-t\mathcal{D}], \Gamma_+\}}{\{\Gamma[-t\mathcal{D}], \Gamma_-\}}. \tag{53}$$

This expression for Θ, which determines the Rényi entropy via Eq. (51), will help us study the purification transition at a quantitative level.

The above considerations help us anticipate the existence of two distinct dynamical phases, consistent with previous work on purification dynamics in discrete time random circuit models, which we refer to as "mixed" ($g < 1$) and "purifying" phases ($g > 1$), following Ref. [34]. In the following, we derive analytical expressions for the time dependence of Θ, which in turn determines the Rényi entropy $\tilde{S}^{(2)}(t)$ via Eq. (51). We will use these expressions later to understand the nature of the two phases and the transition between them at a quantitative level.

B. Expressions for $\Theta(t)$

While we have so far left the boundary conditions unspecified, in computing $\Theta(t)$ we will consider open and periodic boundary conditions separately in our calculations. The conventional timescale $\gamma = 1$ is employed throughout this chapter.

1. Periodic boundary conditions

We start by considering periodic boundary conditions, which can be realized by introducing additional random unitary gates that act between sites 1 and N in the original circuit model. In this case, a standard calculation shows that the Jordan-Wigner-transformed Hamiltonian (39) acquires an additional term which imposes either periodic or antiperiodic boundary conditions depending on the fermion parity sector one works in (see, e.g., Ref. [55]). Taking N to be even from hereon for simplicity, the even (odd) parity sector features antiperiodic (periodic) boundary conditions. These are sometimes referred to as Ramond and Neveu-Schwarz sectors, respectively.

Thanks to the translation invariance of the system, the single particle Hamiltonian $\mathcal{D}$ can be block diagonalized using momentum eigenstates, whose wavevector is quantized to $k_l = l\pi/N$, with $l \in \{1, \ldots, N-1\}$. In the even parity sector l must be odd to be compatible with the boundary conditions, and likewise vice versa. Recognizing that the states $|\pm\rangle$ are the ground states of the Hamiltonian in the $g \to 0$ limit in each parity sector, we can express Θ as a ratio of products over k_l modes, with even l in the numerator and odd l in the denominator. In Appendix V in Ref. [48], we show that

$$\Theta = e^t \frac{\prod_{n=1}^{N/2-1} \theta(k_{2n}, t)}{\prod_{n=1}^{N/2} \theta(k_{2n-1}, t)}, \tag{54}$$

where

$$\theta(k, t) = \cosh(\lambda_k t)\left[1 + \tanh(\lambda_k t)\frac{1 - g\cos k}{\lambda_k}\right], \tag{55}$$

and the energy eigenvalues are given by

$$\lambda_k = \sqrt{1 + g^2 - 2g\cos k}. \tag{56}$$

The factor e^t in Eq. (54) accounts for the modes $k = 0, k = \pi$, which are only present in the odd parity sector.

2. Open boundary conditions

We can also consider open boundary conditions (OBCs), where the Hamiltonian $\mathcal{H}_{\text{eff}}$ no longer features the term connecting sites 1 and N. While the change of boundary condition makes little difference in the purifying phase, we will find that in the mixed phase, quantitative differences between OBCs and PBCs can be seen in the behavior of the Rényi entropy. As such, will focus mainly on mixed phase $g < 1$, although of the following holds true throughout the phase diagram.

With OBCs, the JW-transformed does not contain a term that manifestly depends on the fermion parity sector. This leaves us with the problem of diagonalizing the single-particle matrix $\mathcal{D}$, which is now the same in both parity sectors. Since the system is no longer translation invariant, we cannot treat momentum eigenmodes separately as we did before. Instead, we must explicitly compute the correlation matrices $\Gamma[-t\mathcal{D}]$ and $\Gamma_{\pm}$, and use the more general expression (53). To do so, we calculate the single-particle eigenstates, which form the columns of a real orthogonal eigenvector matrix $\mathcal{O}$. In terms of these, we obtain a spectral decomposition of the grand dynamical matrix $\mathcal{D} = \mathcal{O}\Lambda\mathcal{O}^{-1}$. The eigenvalues Λ come in pairs due to the particle-hole symmetry (41), which we arrange as $\Lambda = \text{diag}(\lambda_0, \lambda_1, \lambda_2, \ldots \lambda_{N-1}, -\lambda_0, -\lambda_1, -\lambda_2, \ldots -\lambda_{N-1})$ with $\lambda_i > 0$ and in nondecreasing order. The corresponding pairs of eigenvectors are also related through $|-\lambda_i\rangle = \eta\,|\lambda_i\rangle$, with η defined in Eq. (41). In terms of these eigenvalues, the correlation matrix $\Gamma[-t\mathcal{D}]$ becomes

$$\Gamma[-t\mathcal{D}] = \mathcal{O}\tanh\left(\frac{-t\Lambda}{2}\right)\mathcal{O}^{-1}, \tag{57}$$

which can be substituted directly into Eq. (53). In Appendix VI in Ref. [48], we show that the single particle eigenstates take the form of sinusoids, whose wavevectors k_l can be found as the solutions to the equation

$$\tan Nk_l = \frac{g\sin k_l}{1 - g\cos k_l}, \tag{58}$$

lying in the interval $[0, \pi)$ and labeled in increasing order. In terms of these wavevectors, the eigenvalues λ_l themselves again follow the well-known dispersion for the TFIM, Eq. (56). In the mixed phase, there is also a single imaginary solution to the above, which we label $k_0 = \mathrm{i}K$, corresponding to a Majorana edge mode localized at the two boundaries of the chain. The energy of this edge mode λ_0 can be shown to be exponentially small in the system size N, and this energy is associated with a long timescale λ_0^{-1} which we will show is responsible for the slow decay of purity in this phase.

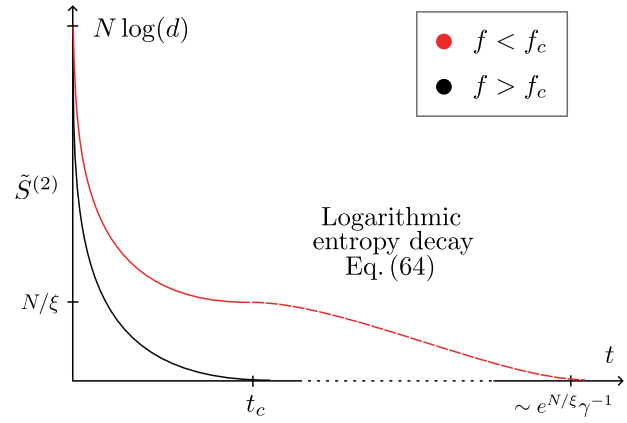

FIG. 2. Qualitative plot showing the behavior of the system entropy on different timescales in the mixed(red) and purifying(black) phase. In the mixing phase, the entropy undergoes a period of very slow logarithmic decay up to exponentially long times in the system size.

C. Behavior of the Rényi entropy

With the above expressions in place, we are now ready to study the behavior of the Rényi entropy in the two phases, as well as the critical point which separates them. A qualitative representation of the findings was given in Fig. 2.

1. Mixed phase—periodic boundary conditions

In the mixed phase, the Rényi entropy shows quantitative differences depending on the boundary conditions, and thus we will consider both PBCs and OBCs in the regime $g < 1$, starting with the former. Beginning with Eq. (54), we can

use complex integration methods to transform the alternating product over even and odd k modes into an infinite product

$$\Theta = \prod_{q=0}^{\infty} \tanh \frac{N x_q}{2}, \tag{59}$$

with x_q's found as the solutions of the equation

$$t\sqrt{2g\cosh x - 1 - g^2} + \phi(x) = \pi\left(q + \frac{1}{2}\right), \tag{60}$$

$$\tan\phi(x) = \frac{g\cosh x - 1}{\sqrt{2g\cosh x - 1 - g^2}}, \tag{61}$$

in the interval (K, ∞), where $K = -\ln g$ is the point in the complex plane where the dispersion function $\lambda(\mathrm{i}K)$ has a zero. This form makes it manifestly clear that $\Theta < 1$. The details of this calculation are given in Appendix V in Ref. [48]. Except at criticality, for sufficiently large N, we can have $NK \gg 1$, which in turn implies $Nx_q \gg 1$ for all q. In this case, by virtue of the approximation $\ln\tanh(y) \approx -2e^{-2y}$ for $y \gg 1$, we can approximate $\ln\Theta$ by an integral

$$\ln\Theta \approx -2\int_K^{\infty} \frac{dq}{dx} e^{-Nx}, \tag{62}$$

where dq/dx is the density of solutions and can be found by differentiating Eq. (60). The result to highest order in powers of N is

$$\ln\Theta(t) = -\sqrt{\frac{1-g^2}{\pi N}} e^{-NK}\left(t + \frac{2}{1-g^2}\right). \tag{63}$$

To relate this expression to the Rényi entropy (15), we focus on the regime where t scales no faster than polynomial in N, such that the small factor e^{-NK} dominates, making $-\ln\Theta(t)$ itself small. Then, if we make the approximations $1 - \Theta \approx -\ln\Theta$ and $1 + \Theta \approx 2$, we can deduce the following form for the Rényi entropy, valid for a broad window of times $e^{NK} \gg t \gg 2/(1-g^2)$ (restoring the original units of time)

$$\tilde{S}^{(2)}(t) = N\ln|g| - \ln\frac{t}{\sqrt{N}} + \frac{1}{2}\ln\frac{4\pi}{1-g^2} + o(1) \tag{64}$$

where the term $o(1)$ represents terms that tend to zero in the limit of large t or N. We see that the entropy decreases very slowly in time in this window, which is a defining feature of the mixed phase.

Finally, for times t that scale exponentially with system size $\gamma t \gtrsim e^{NK}$, such that $|\ln\Theta(t)| \gg 1$, we find that the entropy decays as

$$\tilde{S}^{(2)} \approx 2\Theta(t) \approx 2\exp\left(-\gamma t\sqrt{\frac{1-g^2}{\pi N}} e^{-NK}\right). \tag{65}$$

2. Mixed phase—open boundary conditions

We now wish to compute the same quantity with open boundary conditions in the mixed phase $g < 1$. In particular, we are interested in the regime during which the entropy decays very slowly. As such, we can separate out the bulk single-particle eigenstates, whose energies lie above the bulk gap $\Delta = (1-g)$, from the Majorana edge mode, which is exponentially small in N. In particular, as long as one is not too close to criticality $(1-g) \gg 1/N$, the Majorana eigenvalue can be approximated as

$$\lambda_0 \approx (1-g^2)e^{-NK}. \tag{66}$$

This indicates that there is a regime of times $\Delta^{-1} \ll t \ll \lambda_0^{-1}$ during which the transient bulk modes have decayed away $\exp(-t\lambda_i) \approx 0$, while the Majorana mode has not decayed. The approximate correlation matrix in this regime will then take the form

$$\Gamma[-t\mathcal{D}] = \mathcal{O}\tanh\left(-\frac{t\mathcal{E}}{2}\right)\mathcal{O}^{-1} \approx \mathcal{O}\begin{pmatrix} -\tanh\frac{t\lambda_0}{2} & 0 & 0 & 0 \\ 0 & -I_{N-1} & 0 & 0 \\ 0 & 0 & \tanh\frac{t\lambda_0}{2} & 0 \\ 0 & 0 & 0 & I_{N-1} \end{pmatrix}\mathcal{O}^{-1}. \tag{67}$$

In Appendix VI in Ref. [48], we show that the form of the eigenvectors $\mathcal{O}$ can be found explicitly and the parameter Θ can be expressed using Vandermonde determinants. The factorization of the latter is known, leading to the exact final expression

$$\Theta(t) = e^{-t\lambda_0}\frac{\tanh\frac{NK}{2}\prod_{l\ \mathrm{odd}}(\cosh K - \cos k_l)}{\sinh K\prod_{l\ \mathrm{even}}(\cosh K - \cos k_l)}, \tag{68}$$

where k_l for $1 \leqslant l \leqslant N-1$ are the wavevectors of the bulk modes, defined in Eq. (58), and K is the spatial decay rate of the edge mode. As with the analogous expression for periodic boundary conditions (54), this product can be evaluated with the help of complex integration techniques, which we describe in Appendix VII in Ref. [48]. We find that the large N asymptotic expression of Θ takes the form

$$\ln\Theta(t) = 2e^{-NK}\left(\sqrt{\frac{N}{\pi}}\sqrt{1-g^2} - 1 - \frac{1-g^2}{2}t\right). \tag{69}$$

Again, we focus on the regime where t scales polynomially with N, in which case the right hand side of the above is small. Moreover, noting that Θ should be no greater than unity, we find that the above expression should only be trusted in the regime

$$t \gtrsim t_c = 2\sqrt{\frac{N}{(1-g^2)\pi}}. \tag{70}$$

We view the above constraint as a condition for validity of the approximation (67) made earlier. Then, in this regime we can make the same series of approximations as before to relate $\Theta(t)$ to the Rényi entropy. Thus, for $t_c \lesssim t \ll e^{NK}$, we find

$$\tilde{S}^{(2)}(t) = N\ln|g| - \ln t + \ln\frac{2}{1-g^2} + o(1). \tag{71}$$

At very long times, when t scales exponentially with N such that $|\ln\Theta(t)| \gg 1$, we find that the entropy decays as

$$\tilde{S}^{(2)} \approx 2\exp(-(1-g^2)te^{-NK}). \tag{72}$$

Together, Eqs. (71) and (72) characterize the salient features of purification dynamics in our model in the mixed phase sufficiently far from criticality ($e^{-NK} \ll 1$).

3. Purifying phase

The purifying case corresponds to the regime $g > 1$, where measurements occur so often that they overcome the scrambling and an initially mixed state quickly becomes pure. Looking at the spectrum of the single-particle matrix $\mathcal{D}$, one finds that all eigenvalues are at least as large as the bulk gap $\Delta = (g-1)$, which sets a timescale $t \gtrsim (g-1)^{-1}$ after which the correlation matrix $\Gamma[-t\mathcal{D}]$ will have converged close to its $t \to \infty$ limit.

Using Eq. (59), we see that there is exactly one root x_0 in the interval $0 < x_0 < \ln g$. For large enough N we have that $N \ln g \gg 1$, so for the other roots $\tanh Nx_q/2 \approx 1$. This means that for $t \sim \text{poly}(N)$, we can make the approximation

$$\tilde{S}^{(2)}(t) \approx Nx_0, \tag{73}$$

so x_0 is the entropy density in the chain at time t. The equation determining x_0 can be written as

$$\tanh(t\sqrt{1+g^2-2g\cosh x_0}) = \frac{\sqrt{1+g^2-2g\cosh x_0}}{g\cosh x_0 - 1}. \tag{74}$$

Taking $t \gg 1$ we see that the solution is approximately

$$\tilde{S}^{(2)}(t)/N \approx x_0 \approx \frac{2(g-1)}{g} e^{-t(g-1)} \tag{75}$$

and follows the expected decay rate set by the spectral gap Δ. Since the system is disordered in this regime, the result is expected to hold in the thermodynamic limit, irrespective of the boundary conditions.

4. Critical point

We now address dynamics at the critical point $g = 1$. While we are no longer able to reliably make an approximation of the kind (67) in the open boundary condition case, we find that the purification dynamics for periodic boundary conditions is amenable to analytical treatment in this regime. In particular, Eq. (59) continues to hold at $g = 1$, with the equation for the roots x_q now given as solutions to the equation

$$2t \sinh\frac{x}{2} + \arctan\sinh\frac{x}{2} = \pi\left(q + \frac{1}{2}\right). \tag{76}$$

This equation is still transcendental, making it difficult to find a universal expression for its solutions. However, we can study the three regimes $t \ll 1$, $1 \ll t \ll N$, and $t \gg N$ separately.

Early times $t \ll 1$.—In the initial time frame $t \ll 1$, it can be shown that the entropy is approximately given by

$$\tilde{S}^{(2)} \approx -N \ln\frac{t}{2}. \tag{77}$$

The logarithmic divergence at the origin has a simple intuitive explanation: since the averaging is performed over the purities rather than the entropies and we work in a $d \to \infty$ system, the only scenarios that contribute to the average purity at early times are those where the entire chain is measured. If this happens, the system is immediately purified, since we can neglect the unitary evolution at $t \ll 1$. The entropy is then simply the logarithm of the probability that all qudits are measured within the time t, which is $p \approx (ft)^N = (gt/2)^N$. This intuitive picture matches the exact answer we found above at criticality, and is expected to hold for all values of g in both the periodic and open boundary conditions.

Intermediate times $1 \ll t \ll N$.—In this regime, we can assume $Nx_q \gg 1$ but $x_q \ll 1$ for all solutions x_q that contribute meaningfully to the value of Θ. Using these approximations we find that the x_q are equally spaced and the formula for $\ln\Theta$ is calculated as a geometric sum. The final expression for the entropy is

$$\tilde{S}^{(2)} \approx \frac{N\pi}{2t+1}. \tag{78}$$

The algebraic relationship $\tilde{S}^{(2)} \propto t^{-1}$ is an important feature and only occurs exactly at criticality.

Late times $t \gg N$.—Finally, in the long-time limit, we see that we can approximate Θ by

$$\Theta \approx \frac{(e^{-\frac{N\pi}{2t}}, e^{-\frac{N\pi}{t}})_\infty}{(-e^{-\frac{N\pi}{2t}}, e^{-\frac{N\pi}{t}})_\infty} \approx \sqrt{2}e^{-\frac{\pi t}{4N}}, \tag{79}$$

where $(a,q)_\infty$ is the q-Pochammer symbol. This leads to an exponential decay of the entropy

$$\tilde{S}^{(2)} \approx 2\sqrt{2}e^{-\frac{\pi t}{4N}}. \tag{80}$$

D. Comparison to result from field theory

Having derived expressions for the time dependence of the Rényi entropy of our model of hybrid quantum dynamics, it is instructive to compare our findings to the approach introduced in Ref. [43]. There, the authors invoke an effective field theory known as capillary-wave theory, which was first developed to model the dynamics of domain walls in the low-temperature phase of the Ising model. The correspondence between the two is rooted in the mapping between discrete-time hybrid quantum circuits and two-dimensional ferromagnets, see e.g., Refs. [14,27]. The parameters of the theory are a phenomenological surface tension σ and inverse temperature β, and once these are fixed, it is possible to find approximations for the time dependence of the Rényi entropy starting from a mixed initial state in the associated discrete-time monitored quantum circuit model.

Upon comparing their expression to our results, we find that the same universal features hold. In particular, for both cases, there is a marked regime of times $t \sim \text{poly}(N)$ in the mixed phase during which the entropy decays as an extensive constant with a $-\ln t$ contribution. The sensitivity to boundary conditions we see [Eq. (64) versus (71)] can also be understood in the capillary-wave picture as a consequence of the difference in configurational entropies of the endpoints of a domain wall for periodic versus open boundary conditions. Moreover, by looking at the prefactor of the term proportional to N, we can relate the microscopic parameters of our model to the phenomenological parameters of the field theory; in particular, we can fix the code rate $\beta\sigma = K = -\ln g$, which vanishes nonanalytically at the transition $g = 1$.

VI. DISCUSSION

Our work introduces a class of random unitary circuits following a brickwork geometry, where each unit cell performs an infinitesimally small unitary transformation. We show that the limiting case of the construction above leads to a continuous stochastic process through the many-body Hilbert space. We show that the nonequilibrium behavior of statistical averages of a large class of operator-space entanglement measures (the Rényi entropies) of this dynamical process can be obtained as equilibrium partition functions in an effective quantum spin system, governed by a universal, time-independent Hamiltonian. The construction relies on an initial microscopic Hamiltonian describing local interactions, but we prove that this only enters the effective quantum information dynamics by setting the overall timescale.

We only perform a thorough investigation of the second Rényi entropy, where the effective theory is the spin-1/2 ferromagnetic TFIM, with an integrability breaking term that becomes quadratically small in the local dimension d. The appearance of the Ising model in the 2-replica theory is not unique to the continuous-time model studied here, but is also found in discrete models. A central difference is that discrete models lead to 2d classical Ising models on triangular lattices [17,19]. This shares similar critical characteristics with the TFIM found here, but makes properties away from criticality more difficult to obtain.

The ground state of the effective theory becomes degenerate in the thermodynamic limit and it is ferromagnetically ordered. Taking a phenomenological perspective, the two types of stable ordering roughly correspond to the measuring agent having full knowledge or no knowledge about the state of the system. The lowest energy excitations are topological domain walls, and roughly represent the geometric boundaries of our knowledge. We show that local measurements can also be studied within the same framework by adding an extra state to the spins of the effective system. When the local tumbling rate of the microscopic Hamiltonian is sufficiently strong, this extra state is adiabatically eliminated, and the effect of measurements is to introduce a transverse magnetic field whose strength is proportional to the measurement frequency. When this exceeds a critical threshold, the system undergoes an Ising-type phase transition into a disordered phase. This is recognized as the purification transition observed in numerical studies of similar models [34,36]. The signature of the transition is a logarithmically decaying residual uncertainty in the state of the system after a purification procedure using uncorrelated local measurements, which is present only if the system is in the ordered phase.

We identify the order parameter corresponding to the residual second Rényi entropy in the effective model and prove exact product expansion formulas that can be used to calculate it in both open and closed boundary conditions. Complex integration techniques are used to find thermodynamic limit approximations on various timescales, and we see that their scaling agrees with field theoretic arguments. The method is not restricted to the residual entropy of the whole chain, and could be adapted to calculations of other second Rényi entropies. Universal characteristics of the transition such as the critical exponents must be the same as for the effective 1D quantum Ising theory. The transition in the von Neumann entropy requires higher replica analysis and may be of a different universality class, but we expect a qualitatively similar behavior away from criticality. We begin the investigation of higher replica calculations by proving a formula for the matrix elements of the effective Hamiltonian in Appendix II in Ref. [48]. In contrast with similar models based on discrete evolution studied in literature, our circuits are not expected to lead to a percolation transition of the von Neumann entropy, even in the $d \to \infty$ limit. This is because the small gate action limit $\Delta t \to 0$ is taken first, making the Hartley entropy S_0 undefined for any d.

To simplify our calculations, we have set the local tumbling rate Γ to infinity, but it may be interesting to investigate how it affects the transition. This introduces measurement inertia, wherein less information is gained by consecutively measuring the same qudit at intervals less than $\sim 1/\Gamma$. If the measurement frequency grows beyond this, the qudits become effectively Zeno-locked. To the best of our knowledge, the growth of entanglement in this regime has not been previously investigated.

From an experimental perspective, the large tumbling rate limit of the model introduced here can be expected in physical systems whenever the state of local spins is scrambled on timescales much larger than those of interspin interactions. Our theory predicts universal features of entanglement dynamics in this regime, irrespective of the nature of the local interactions.

ACKNOWLEDGMENTS

This work was supported in part by EPSRC Grant EP/S020527/1. S.L. acknowledges support from UCL's Graduate Research Scholarship and Overseas Research Scholarship. M.M. acknowledges support from Trinity College, Cambridge.

[1] P. Calabrese and J. Cardy, Evolution of entanglement entropy in one-dimensional systems, J. Stat. Mech. (2005) P04010.

[2] H. Kim and D. A. Huse, Ballistic spreading of entanglement in a diffusive nonintegrable system, Phys. Rev. Lett. **111**, 127205 (2013).

[3] W. W. Ho and D. A. Abanin, Entanglement dynamics in quantum many-body systems, Phys. Rev. B **95**, 094302 (2017).

[4] P. Calabrese and J. Cardy, Entanglement entropy and conformal field theory, J. Phys. A: Math. Theor. **42**, 504005 (2009).

[5] P. Hosur, X.-L. Qi, D. A. Roberts, and B. Yoshida, Chaos in quantum channels, J. High Energy Phys. 02 (2016) 004.

[6] A. Nahum, J. Ruhman, S. Vijay, and J. Haah, Quantum entanglement growth under random unitary dynamics, Phys. Rev. X **7**, 031016 (2017).

[7] T. Zhou and A. Nahum, Emergent statistical mechanics of entanglement in random unitary circuits, Phys. Rev. B **99**, 174205 (2019).

[8] A. Chan, A. De Luca, and J. T. Chalker, Solution of a minimal model for many-body quantum chaos, Phys. Rev. X **8**, 041019 (2018).

[9] D. A. Roberts and B. Yoshida, Chaos and complexity by design, J. High Energy Phys. 04 (2017) 121.

[10] A. Nahum, S. Vijay, and J. Haah, Operator spreading in random unitary circuits, Phys. Rev. X **8**, 021014 (2018).

[11] C. W. von Keyserlingk, T. Rakovszky, F. Pollmann, and S. L. Sondhi, Operator hydrodynamics, otocs, and entanglement growth in systems without conservation laws, Phys. Rev. X **8**, 021013 (2018).

[12] T. Rakovszky, F. Pollmann, and C. W. von Keyserlingk, Diffusive hydrodynamics of out-of-time-ordered correlators with charge conservation, Phys. Rev. X **8**, 031058 (2018).

[13] Y. Li, X. Chen, and M. P. A. Fisher, Quantum zeno effect and the many-body entanglement transition, Phys. Rev. B **98**, 205136 (2018).

[14] B. Skinner, J. Ruhman, and A. Nahum, Measurement-induced phase transitions in the dynamics of entanglement, Phys. Rev. X **9**, 031009 (2019).

[15] A. Chan, R. M. Nandkishore, M. Pretko, and G. Smith, Unitary-projective entanglement dynamics, Phys. Rev. B **99**, 224307 (2019).

[16] Y. Li, X. Chen, and M. P. A. Fisher, Measurement-driven entanglement transition in hybrid quantum circuits, Phys. Rev. B **100**, 134306 (2019).

[17] Y. Bao, S. Choi, and E. Altman, Theory of the phase transition in random unitary circuits with measurements, Phys. Rev. B **101**, 104301 (2020).

[18] S. Choi, Y. Bao, X.-L. Qi, and E. Altman, Quantum error correction in scrambling dynamics and measurement-induced phase transition, Phys. Rev. Lett. **125**, 030505 (2020).

[19] C.-M. Jian, Y.-Z. You, R. Vasseur, and A. W. W. Ludwig, Measurement-induced criticality in random quantum circuits, Phys. Rev. B **101**, 104302 (2020).

[20] A. Zabalo, M. J. Gullans, J. H. Wilson, S. Gopalakrishnan, D. A. Huse, and J. H. Pixley, Critical properties of the measurement-induced transition in random quantum circuits, Phys. Rev. B **101**, 060301(R) (2020).

[21] A. Nahum, S. Roy, B. Skinner, and J. Ruhman, Measurement and entanglement phase transitions in all-to-all quantum circuits, on quantum trees, and in landau-ginsburg theory, PRX Quantum **2**, 010352 (2021).

[22] M. Ippoliti, M. J. Gullans, S. Gopalakrishnan, D. A. Huse, and V. Khemani, Entanglement phase transitions in measurement-only dynamics, Phys. Rev. X **11**, 011030 (2021).

[23] A. Zabalo, M. J. Gullans, J. H. Wilson, R. Vasseur, A. W. W. Ludwig, S. Gopalakrishnan, D. A. Huse, and J. H. Pixley, Operator scaling dimensions and multifractality at measurement-induced transitions, Phys. Rev. Lett. **128**, 050602 (2022).

[24] A. J. Friedman, O. Hart, and R. Nandkishore, Measurement-induced phases of matter require feedback, PRX Quantum **4**, 040309 (2023).

[25] R. Vasseur, A. C. Potter, Y.-Z. You, and A. W. W. Ludwig, Entanglement transitions from holographic random tensor networks, Phys. Rev. B **100**, 134203 (2019).

[26] P. Hayden, S. Nezami, X.-L. Qi, N. Thomas, M. Walter, and Z. Yang, Holographic duality from random tensor networks, J. High Energy Phys. 11 (2016) 009.

[27] N. Bao, G. Penington, J. Sorce, and A. C. Wall, Beyond toy models: Distilling tensor networks in full ads/cft, J. High Energy Phys. 11 (2019) 069.

[28] Z.-C. Yang, Y. Li, M. P. A. Fisher, and X. Chen, Entanglement phase transitions in random stabilizer tensor networks, Phys. Rev. B **105**, 104306 (2022).

[29] O. Alberton, M. Buchhold, and S. Diehl, Entanglement transition in a monitored free-fermion chain: From extended criticality to area law, Phys. Rev. Lett. **126**, 170602 (2021).

[30] H. Lóio, A. De Luca, J. De Nardis, and X. Turkeshi, Purification timescales in monitored fermions, Phys. Rev. B **108**, L020306 (2023).

[31] X. Chen, Y. Li, M. P. A. Fisher, and A. Lucas, Emergent conformal symmetry in nonunitary random dynamics of free fermions, Phys. Rev. Res. **2**, 033017 (2020).

[32] M. Szyniszewski, A. Romito, and H. Schomerus, Entanglement transition from variable-strength weak measurements, Phys. Rev. B **100**, 064204 (2019).

[33] X. Cao, A. Tilloy, and A. D. Luca, Entanglement in a fermion chain under continuous monitoring, SciPost Phys. **7**, 024 (2019).

[34] M. J. Gullans and D. A. Huse, Dynamical purification phase transition induced by quantum measurements, Phys. Rev. X **10**, 041020 (2020).

[35] M. J. Gullans and D. A. Huse, Scalable probes of measurement-induced criticality, Phys. Rev. Lett. **125**, 070606 (2020).

[36] S. Gopalakrishnan and M. J. Gullans, Entanglement and purification transitions in non-hermitian quantum mechanics, Phys. Rev. Lett. **126**, 170503 (2021).

[37] C. Noel, P. Niroula, D. Zhu, A. Risinger, L. Egan, D. Biswas, M. Cetina, A. V. Gorshkov, M. J. Gullans, D. A. Huse, and C. Monroe, Measurement-induced quantum phases realized in a trapped-ion quantum computer, Nat. Phys. **18**, 760 (2022).

[38] R. Fan, S. Vijay, A. Vishwanath, and Y.-Z. You, Self-organized error correction in random unitary circuits with measurement, Phys. Rev. B **103**, 174309 (2021).

[39] T. Vovk and H. Pichler, Entanglement-optimal trajectories of many-body quantum markov processes, Phys. Rev. Lett. **128**, 243601 (2022).

[40] F. Azad, A. Hallam, J. Morley, and A. G. Green, Phase transitions in the classical simulability of open quantum systems, Sci. Rep. **13**, 8866 (2023).

[41] Z. Chen, Y. Bao, and S. Choi, Optimized trajectory unraveling for classical simulation of noisy quantum dynamics, arXiv:2306.17161 [quant-ph].

[42] Z. Cheng and M. Ippoliti, Efficient sampling of noisy shallow circuits via monitored unraveling, PRX Quantum **4**, 040326 (2023).

[43] Y. Li and M. P. A. Fisher, Statistical mechanics of quantum error correcting codes, Phys. Rev. B **103**, 104306 (2021).

[44] M. Szyniszewski, A. Romito, and H. Schomerus, Universality of entanglement transitions from stroboscopic to continuous measurements, Phys. Rev. Lett. **125**, 210602 (2020).

[45] M. Jiang, S. Luo, and S. Fu, Channel-state duality, Phys. Rev. A **87**, 022310 (2013).

[46] Y. Bao, M. Block, and E. Altman, Finite time teleportation phase transition in random quantum circuits, arXiv:2110.06963.

[47] E. Bianchi, L. Hackl, and N. Yokomizo, Linear growth of the entanglement entropy and the kolmogorov-sinai rate, J. High Energy Phys. 03 (2018) 025.

[48] See Supplemental Material at http://link.aps.org/supplemental/10.1103/PhysRevB.108.174308 for calculations of the effective Hamiltonians, evolution of the X state, connection between the effective and microscopic Hamiltonians and explicit calculation of the entropy in open and closed boundary conditions.

[49] H. Hinrichsen, Non-equilibrium critical phenomena and phase transitions into absorbing states, Adv. Phys. **49**, 815 (2000).

[50] M. N. Barber and P. M. Duxbury, A quantum hamiltonian approach to the two-dimensional axial next-nearest-neighbour ising model, J. Phys. A: Math. Gen. **14**, L251 (1981).

[51] W. Selke, The annni model–theoretical analysis and experimental application, Phys. Rep. **170**, 213 (1988).

[52] I. Mahyaeh and E. Ardonne, Study of the phase diagram of the kitaev-hubbard chain, Phys. Rev. B **101**, 085125 (2020).

[53] A. Maiellaro, A. Marino, and F. Illuminati, Topological squashed entanglement: Nonlocal order parameter for one-dimensional topological superconductors, Phys. Rev. Res. **4**, 033088 (2022).

[54] D. Gottesman, Fault-tolerant quantum computation with higher-dimensional systems, Chaos, Solitons & Fractals **10**, 1749 (1999).

[55] G. B. Mbeng, A. Russomanno, and G. E. Santoro, The quantum ising chain for beginners, arXiv:2009.09208 [quant-ph].

[56] A. Y. Kitaev, Unpaired majorana fermions in quantum wires, Phys. Usp. **44**, 131 (2001).

[57] M. Fagotti and P. Calabrese, Entanglement entropy of two disjoint blocks in xy chains, J. Stat. Mech. (2010) P04016.

[58] M. Heyl, A. Polkovnikov, and S. Kehrein, Dynamical quantum phase transitions in the transverse-field ising model, Phys. Rev. Lett. **110**, 135704 (2013).

[59] M. Heyl, Dynamical quantum phase transitions: A review, Rep. Prog. Phys. **81**, 054001 (2018).